Archaeometric Characterisation and Assessment of Conservation State of Coins: The Case-Study of a Selection of Antoniniani from the Hoard of Cumae (Campania Region, Southern Italy)

Sabrina Pagano, Giuseppina Balassone, Chiara Germinario, Celestino Grifa, Francesco Izzo, Mariano Mercurio, Priscilla Munzi, Lucia Pappalardo, Emanuela Spagnoli, Maria Verde, et al.

heritage

MDPI

Article

Archaeometric Characterisation and Assessment of Conservation State of Coins: The Case-Study of a Selection of Antoniniani from the Hoard of Cumae (Campania Region, Southern Italy)

Sabrina Pagano [1,2,*], Giuseppina Balassone [3,4,5], Chiara Germinario [1], Celestino Grifa [1,4], Francesco Izzo [3,4], Mariano Mercurio [1,4], Priscilla Munzi [6], Lucia Pappalardo [5], Emanuela Spagnoli [7], Maria Verde [3] and Alberto De Bonis [3,4]

1 Dipartimento di Scienze e Tecnologie, Università Degli Studi del Sannio, Via Francesco De Sanctis, 82100 Benevento, Italy
2 Dipartimento di Scienze Dell'antichità, Università Degli Studi di Roma La Sapienza, Piazzale Aldo Moro 5, 00185 Roma, Italy
3 Dipartimento di Scienze Della Terra, Dell'ambiente e Delle Risorse (DiSTAR), Università degli Studi di Napoli Federico II, Complesso Universitario di Monte Sant'Angelo, Via Cintia 21, 80126 Napoli, Italy
4 CRACS, Center for Research on Archaeometry and Conservation Science, Complesso Universitario di Monte Sant'Angelo, Via Cupa Nuova Cintia 21, 80126 Napoli, Italy
5 Istituto Nazionale di Geofisica e Vulcanologia, Osservatorio Vesuviano, Via Diocleziano 328, 80124 Napoli, Italy
6 Centre Jean Bérard, UAR3133, CNRS—EFR, Via Francesco Crispi 86, 80121 Napoli, Italy
7 Dipartimento di Studi Umanistici, Università di Napoli Federico II, Via Porta di Massa 1, 80133 Napoli, Italy
* Correspondence: sabrina.pagano@unisannio.it

Abstract: The paper presents the first archaeometric results on a selection of ancient Roman coins (antoniniani) from a treasure found in the Roman necropolis area of ancient Cumae (Southern Italy) during archaeological campaigns by the Centre Jean Bérard. A multi-analytical approach consisting of non-destructive techniques (stereomicroscopy, FESEM-EDS, pXRF, Raman, μ-CT) was implemented on the better-preserved coins of the treasure in order to investigate the chemical composition of the alloy. Chemical analysis showed that the Roman mint prepared the metal with an argentiferous lead–bronze alloy. A group of coins presents a low content of the precious metal, which is in agreement with the financial crisis of the Roman Empire of the third century. Another group of two coins shows a higher silver content, which is in agreement with their issue or with the Mediolanum mint standards. In addition, the external layers of corroded coins were analysed to explore the state of conservation of the patina and to identify the corrosion products. Some typical corrosion patinas due to post-depositional conditions were identified. The mineralogical characterisation of the corrosion products enables us to implement adequate conservation strategies, and the presence of more aggressive patinas suggests immediate interventions.

Keywords: Roman imperial coinage; antoniniani; Cumae; metals; alloy composition; spectroscopy; corrosion products; patinas

Citation: Pagano, S.; Balassone, G.; Germinario, C.; Grifa, C.; Izzo, F.; Mercurio, M.; Munzi, P.; Pappalardo, L.; Spagnoli, E.; Verde, M.; et al. Archaeometric Characterisation and Assessment of Conservation State of Coins: The Case-Study of a Selection of Antoniniani from the Hoard of Cumae (Campania Region, Southern Italy). *Heritage* **2023**, *6*, 2038–2055. https://doi.org/10.3390/heritage6020110

Academic Editors: Fabrizio Antonelli, Chiara Coletti, Luigi Germinario and Elena Tesser

Received: 31 December 2022
Revised: 12 February 2023
Accepted: 14 February 2023
Published: 16 February 2023

1. Introduction

The great interest of ancient coins arises both from their aesthetic value and from the historical, economic, archaeological and technological information that they provide. Coins become a wide-ranging documentary source and their analytical studies represent a relevant contribution to the archaeological and numismatic research to answer questions of different natures (i.e., raw material, provenance, technological skills, economic trend) [1–5]. Information on their chemical composition can provide indications on the level of metallurgical technology and the precious metal standards established by the mints under the

control of Rome [6–9]. Outer layer compositional data can also aid in coin authentication and shed light on monetary issues of which no record in historical sources is available [10].

Early studies carried out on metals, particularly on coined metals, were performed with highly invasive methodologies [11]. By the middle of the last century, non-invasive spectroscopic techniques became a valuable tool for the archaeometric evaluation of archaeological materials, with the purpose of preserving their integrity. Indeed, most of the studies performed in the field of cultural heritage do not permit the performance of destructive analyses and, therefore, non-invasive and non-destructive techniques represent a useful method for the characterisation of these materials [12]. However, archaeological materials often undergo burial processes that induce modifications in terms of morphology and chemical composition. On the basis of their original composition and the environment in which they were buried, the metal finds have different corrosion materials on the surface [13,14]. The exchange of ions between the less noble elements of the alloy and the constituent elements of the soil causes a surface enrichment in silver-bearing bronze coins which induces an overestimation of the fineness content [15]. For these reasons, there are several studies concerning the characterisation of the external layer and its corrosion products, while few studies can be carried out on the metal core which preserves the original alloy [15–17].

The necessary condition to have a reliable investigation is the homogeneity of the surface, which is difficult to have on objects that have been buried for a long time and which must not be further altered by diagnostic analyses. For this reason, a semi-quantitative significance is often assigned to portable X-ray fluorescence (pXRF) surface analyses [18]. Several authors have tried to use the pXRF technique for the chemical analysis of the alloy composition, in part because it consists of portable instrument that can be easily transported into the museums where ancient monetary collections are kept [19–23]. Nevertheless, recent studies have shown that the chemical composition of metals with patinas up to 25 μm thick can be satisfactorily investigated with pXRF instrumentation [24]. It means that up to that level, the effects of corrosion are not strong enough to alter the values of the main elements [24,25]. Along with the X-ray fluorescence technique, the Raman spectroscopy is commonly used for non-destructive and non-invasive analysis on ancient coins [26–28], as well as the scanning electron microscopy/energy dispersive X-ray spectrometry (SEM-EDS) [29–31] sometimes combined with an electron micro probe analyser (EMPA) [15,31–33]. Micro-invasive analyses carried out by a field emission scanning electron microscope with a focused ion beam (FIB-FESEM-EDS) may provide useful information on the microstructure and corrosion processes [32,34]. Electrochemical techniques (i.e., cyclic voltammetry and electrochemical impedance spectroscopy) have also found wide application in the characterisation and monitoring of metal artefacts [35,36].

This study is based on the archaeometric examination of a selection of coins operated under the responsibility of E. Spagnoli and P. Munzi, from a treasure excavated in the ancient Cumae (Campania region, Southern Italy) by the Centre Jean Bérard team of Naples. The treasure has a great significance since in the Campania region and in the coastal area, there are few numismatic finds coming from well-documented contexts, with the exception of Paestum [37]. The first archaeometric results are discussed in this study (concerning the numismatic study, refer to the forthcoming monography edited by E. Spagnoli). The archaeological coins here presented were studied to define the morphology and the elemental composition and to evaluate their state of conservation via the detection of the different corrosion products. Due to the high historical importance of the find, a non-destructive analytical approach was performed (stereomicroscopy, pXRF, μ-CT imaging, Raman spectroscopy and FESEM-EDS). The information acquired from the archaeometric characterisation may allow the archaeologist and numismatist to place the archaeological finds in a wider cognitive dimension, but these data are also able to provide valid indications to conservators; in fact, better knowledge of the artefact and its state of conservation may assist the implementation of adequate conservation strategies in order to safeguard the cultural heritage [38].

2. Archaeological–Historical Outlines

The ancient city of Cumae (Campania region, Southern Italy) has returned a significant heritage of artifacts and knowledge of the ancient world [39]. For almost thirty years, various institutions have been engaged in the excavations of Cumae within the multi-year Kyme project for the exploration of the city and the necropolis, the latter investigated by the French Institute Centre Jean Bérard (CJB) [40,41]. Among the areas brought to light by the archaeologist of the CJB, the Area 63 (Figure 1a,b) pertains to the Monumento funerario della Sfinge, dated back to the 1st century CE, of which at least four construction phases are known [42]. This is an area that underwent various transformations during the 1st century CE up to the partial obliteration of the monument with the construction of the road via Domiziana (95 CE) and the reuse of some blocks in the construction of the road [42]. During the 3rd century CE, the western area of the complex was used for craft activities [43], as evidenced by the presence of tanks and an aquifer collection well, while the eastern area maintained its funerary use. During the excavation campaign in the western sector, in the area adjacent to the filling well (Figure 1c,d), a chronologically homogeneous treasure was found, consisting of 63 Roman coins [44].

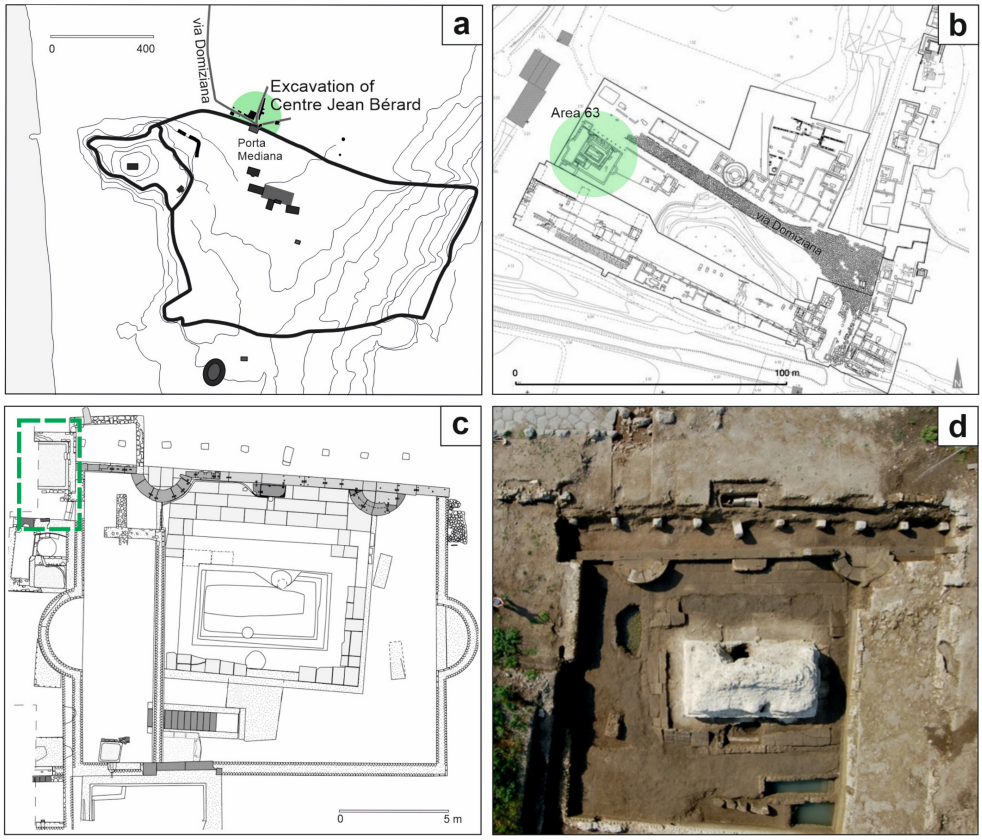

Figure 1. (**a**) Sketch map of ancient city of Cumae (the excavations of the Centre Jean Bérard are highlighted in green) (modified from [45]); (**b**) indication of the Area 63 (in green) in the plan of the CJB excavations of the necropolis area (modified from [46]); (**c**) plan and (**d**) aerial photography of the Area 63 in which the treasure was buried (indicated in the green box) (modified from [45]).

These coins also allowed for setting the date of the abandonment of the area to 270–271 CE, following a natural catastrophic event, probably an earthquake [37,47].

The coins that make up the treasure are antoniniani. The term antoninianus was used in the *Historia Augusta* to define the coin and wastaken from the name of the Emperor Marcus Aurelius Antoninus, known as Caracalla, who introduced this type of coin in 215 CE [48–50]. The term was then revived in modern times and the coin also was given

the name of radiati for the radiated head with which the Emperors are depicted, but the ancient name of the coin is unknown.

The coins of the treasure were issued in a limited time span ranging from 260 to 270 CE [37]. In this period Publius Licinius Egnatius Gallienus (253–268 CE) reigned in Rome and issued coins, succeeded by the Illyrian Emperor Marcus Aurelius Flavius Valerius Claudius, known as Claudius II the Gothic (268–270 CE) [37,51]. The Roman Empire was in a period of strong instability due to the political crisis, but also and above all an economic and 'financial crisis of the 3rd century' [52]. The Emperors were forced to resort to the debasement of coinage to heal the coffers of the Empire by lowering the content of the precious metal [53]. In fact, the coinage was continuously modified in its intrinsic value.

The monetary crisis is clear in the antoniniano phase and thus in the examined coins [54]. Since its issuance and up to 274 CE, with the Aurelian reform, antoninianus coins underwent a continuous decrease in the silver content, more drastically with Valerianus and his son Gallienus and with a major depression with Claudius II in 270 CE [55]. Antoninianus coins continued to be issued until the end of the 3rd century CE.

3. Materials and Methods

3.1. Sampling

The treasure consists of 63 antoniniani minted between the Gallienus' empire and the beginning of Aurelianus' empire. For the present work, 20 coins (Figure 2) have been selected and examined with non-invasive and non-destructive techniques.

Figure 2. Selection of twenty coins analysed (obverse and reverse for each sample).

Considering the different monetary attributions of the coins, 12 coins (#6, #18, #28, #30, #33, #35, #41, #52, #53, #56, #57, #60) of Gallienus, which also appear in greater numbers in the whole treasury, 3 coins (#01, #40, #47) of Claudius II the Gothic and 5 coins (#5, #22, #37, #44, #62) of consecration to Divo Claudio have been selected (Table 1). The selection covers a chronological period of just over ten years, from 260 to 270 CE, approximately. The analysed coins were struck by the mint of Rome, except for two coins struck by the mint of Medionalum (ancient Milan): the coin #47 (issued by *Claudius II*) and the coin #53 (issued by Gallienus), the latter belonging to the series of "legionary coins".

Table 1. Macroscopic and historical features of 20 analysed coins.

n.	Coins	Issuing Authority	Classification	Mint	Diameter (mm)	Weight (g)
1.	**#01**	*Claudius II*	RIC V.1/2, 91, RIC temp #288	Rome	21.5	2.5
2.	**#05**	* *Divo Claudio*	RIC V.1/2, 261, RIC temp #1275	Rome	19.5	2.2
3.	**#06**	*Gallienus*	RIC V.1, 285	Rome	19.5	3.4
4.	**#18**	*Gallienus*	RIC V.1, 207	Rome	21	3.9
5.	**#22**	* *Divo Claudio*	RIC V.1/2, 261, RIC temp #1276	Rome	19	2.8
6.	**#28**	*Gallienus*	RIC V.1, 176	Rome	19.5	3.7
7.	**#30**	*Gallienus*	RIC V, 193	Rome	18.5	2.1
8.	**#33**	*Gallienus*	RIC V.1, 230	Rome	22.5	3.2
9.	**#35**	*Gallienus*	RIC V.1, 177	Rome	18.5	2.8
10.	**#37**	* *Divo Claudio*	RIC V.1/2, 261, RIC temp #1275	Rome	22	2.4
11.	**#40**	*Claudius II*	RIC V,1/2, 45; RIC temp #192	Rome	20	6.0
12.	**#41**	*Gallienus*	RIC V.1, 163 cfr	Rome	19 × 24	3.6
13.	**#44**	* *Divo Claudio*	RIC V.1/2, 261, RIC temp #1275	Rome	21.5	4.1
14.	**#47**	*Claudius II*	RIC V.1/2, 171; RIC temp #33	Mediolanum	19.5	4.3
15.	**#52**	*Gallienus*	RIC V.1, 32	Rome	19.5 × 23.5	3.6
16.	**#53**	*Gallienus*	RIC V.1, 478 cfr.	Mediolanum	21	2.6
17.	**#56**	*Gallienus*	RIC V.1, 207	Rome	21.5	3.1
18.	**#57**	*Gallienus*	RIC V.1, 207	Rome	19.8	4.1
19.	**#60**	*Gallienus*	RIC V, I, 282 cfr.	Rome	20	3.1
20.	**#62**	* *Divo Claudio*	RIC V.1/2, 261, RIC temp #1275	Rome	21.5	2.4

Legend: the asterisk (*) indicates the consecration coins issued for Claudius II. The numbering of the samples is based on the CJB excavation inventory, and the numismatic classification is taken from the forthcoming publication of E. Spagnoli.

3.2. Methods

To evaluate the composition, the structure and the damage of the coins, various analytical steps from macro-to-micro were carried out. In order to perform the analyses in a completely non-destructive way, no cleaning treatments were performed on the coins.

At first, the observation was carried out with the Nikon SMZ-1500 binocular stereomicroscope with HR Plan Apochromat 1x apochromatic objective. The instrumentation has a built-in Digital Sight DS-SM camera and Digital Sight DS-L1 monitor and is equipped with a two-arm Photonic PL2000 adjustable lamp. The microscopic lenses offer magnifications that cover a range from 0.75× to 11.25×.

All samples were subjected to pXRF analysis with portable instrumentation to determine the chemical composition of the coins. Measurements were performed with a Bruker portable spectrometer Tracer 5G, which consists of an X-ray generator with a rhodium (Rh) anode. The SDD detector has a 20mm^2 wide active area with graphene window and an internal camera. The diameter of the spot at the measuring point is 3 mm. The analyses were performed by varying the acquisition conditions defined by voltage (kV), current (μA) and time (s). Each coin was analysed on the two sides by a total of six measurements. On each face of the coins, one measurement was performed with the Std. Alloy3 HighZ preset (40 kV, 37 μA, 60 s) and one with the Std. Alloy3 LowZ preset (15 kV, 16 μA, 60 s). The different pXRF spectral acquisition settings have made it possible to better identify elements with a high atomic number or the main constituents of the alloy, but also those with a low atomic number attributable to the alterations. In addition, one measurement on each face of the coins was carried out with the Precious Metals 2 (PM2; 40 kV, 8 μA, 15 s) application of the instrument that allowed for a quantitative chemical analysis of the

investigated area with the percentage concentrations of the elements composing the alloy. The spectra were processed using the ARTAX software. By comparing the spectra with an internal database, the application verifies any correspondence with known metal alloys. The preliminary verification of the calibration of the instrument was carried out with a standard sample of sterling silver.

Surface corrosion products were analysed using the hand-held spectrometer Bruker BRAVO (Bruker Raman Verification Optics) equipped with a fibre optic probe to analyse specific areas of the sample and a high quantum efficiency array CCD detector to ensure a good signal-to-noise ratio in the acquired spectra. The spectrometer provides a spectral resolution of 10–12 cm^{-1} and features a double laser excitation with different wavelengths (Duo LASER ™) and benefits from a patented SSE ™ (Sequentially Shifted Excitation) technology capable of mitigating the phenomena of fluorescence [56]. The lasers simultaneously affect the sample, resulting in high sensitivity over a wide spectral range from 178 cm^{-1} to 3200 cm^{-1}. Data acquisition and processing was carried out with the OPUS 7.0 software. The identification of the spectra was carried out by comparing the RRUFF reference database [57] and further references were obtained from the literature data [58].

Based on morphological and chemical characteristics, 13 representative coins were selected for the FESEM-EDS analyses performed by a Zeiss Merlin VP FESEM (Field Emission Scanning Electron Microscope) microscope, equipped with a large Gemini II working chamber, which allowed the coins to be inserted directly into the sample chamber. It is equipped with an Oxford EDS X-Max spectrometer. The samples were investigated in both SE and BSE modes working on variable pressure and the images were recorded at different acceleration voltages in the range from 3 to 10 kV with 10 seconds for acquisition and at different working distances. Digital Image Analysis (DIA) was processed with ImageJ software (public Java domain image processing) in order to distinguish different areas on the basis of the chemical composition derived by the SEM/EDS analysis. From the total area captured in BSE, Ag-rich areas were subtracted to estimate their distribution. Segmented and total areas were calculated by software in microns and subsequently converted to percentage values.

For the visualisation of the 3D internal microstructure (pores, cracks) of coins X-ray computed microtomography (μ-CT), analyses were conducted at the OV-INGV (Osservatorio Vesuviano—Istituto Nazionale di Geofisica e Vulcanologia) of Naples on a selection of six coins chosen on the basis of the monetary attribution, the different mints and their state of conservation. In this study, microtomographic analyses have been performed using a Carl Zeiss Xradia Versa-410 3D X-ray microscope. This system includes a polychromatic microfocus X-ray source (40–150 kV, maximum 10 W) for canning the samples with a wide density range and 2 k × 2 k pixel, noise suppressed charge-coupled detector equipped with different magnification objectives (0.4×, 4×, 10×, 20×) that allow a high resolution up to 0.9 μm/voxel. Coins were scanned in absorption mode, acquiring 4001 projections over a 360° rotation at 90–80 kV and 8–7 W with objective 4x.

4. Results and Discussion

4.1. Chemical Composition

To identify the chemical composition, pXRF and FESEM-EDS analyses were performed on the surface of the coins [59]. Since the pXRF method is basically a surface analytical technique [15,23], the compositional assessment of the alloy has been carried out on better preserved coins, showing a less diffuse corrosion. Therefore, the measurements (Std. Alloy3 HighZ preset) focused on coins areas that were not affected by patinas [25]. Nonetheless, measurements on more altered coins (#5, #6, #30, #41, #47, #57, #62: Figure 2) were carried out in order to better define the corrosion products affecting the surfaces. Although the qualitative data are easily available from the interpretation of the spectra, it was not possible to obtain quantitative information by FESEM-EDS because these measurements were carried out working under Variable Pressure.

Table 2 reports the chemical composition of the main elements composing the alloy obtained by PM2 application. Data obtained do not include elements attributable to the contaminations that were detected in the spectra.

Table 2. Precious Metals2 results showing the prevalent elements of the analysed coins.

Issuing Authority	ID Sample	Ag (%)	Cu (%)	Pb (%)	Sn (%)
Gallienus	#18	3	84	7	6
	#28	3	75	16	6
	#33	4	80	11	4
	#35	3	80	10	7
	#52	17	72	9	1
	#53	16	80	4	0
	#56	4	73	13	9
	#60	3	74	18	5
Claudius II	#1	2	73	16	9
	#40	2	71	23	4
Divo Claudio	#22	3	77	15	4
	#37	4	91	4	1
	#44	3	71	20	6

4.1.1. *Gallienus* Coins

The analysed coins issued by the Emperor Gallienus (coins #18, #28, #33, #35, #52, #53, #56, #60: Figure 2) show an overall homogeneous composition (Figure 3), except for two samples (coins #52 and #53: Figure 3). pXRF spectra detected major content of copper, silver, tin and lead along with minor content of iron, calcium and traces of nickel (Figure 3), and EDS analyses confirmed this composition, highlighting different areas in which the elements concentrate themselves (Figure 4). Copper, lead, silver and tin represent the main elements of alloy composition (Table 2); the other elements refer to the alterations intended both as impurities of the alloy and as contamination of the soil in which they are lying [17].

Therefore, a bronze alloy characterised by a high lead content and a limited addition of silver was used to produce these coins. Lead was frequently used in copper alloys and the high lead content suggests a voluntary addition, excluding its accidental occurrence due to the use of galena argentifera for the extraction of silver [60,61]. Lead was added for technological reasons, as it improved their fluidity lowering the melting point of the alloy, but also for logistic–economic reasons. Indeed, due to great availability of lead in territories under the Roman control (i.e., the Italic peninsula), this was a cheap metal, while the tin deposits were located in territories where the Roman power was collapsing (i.e., the Iberian peninsula) [33]. As far as the other chemical elements detected are concerned, they can be attributed to the soil where the coins were buried. However, the presence of iron could be also assumed as an impurity of the metal, considering that its peaks were always detected. Iron was not added voluntarily to the bronze alloy, so its presence could be traced back to the fusion of Fe-rich copper minerals, such as chalcopyrite ($CuFeS_2$) [33,62]. The low silver content, which often represents the main focus of numismatists, should be quite consistent with historical sources on the Gallienus coinage, according to which the content of precious metal is drastically reduced in those years [63,64].

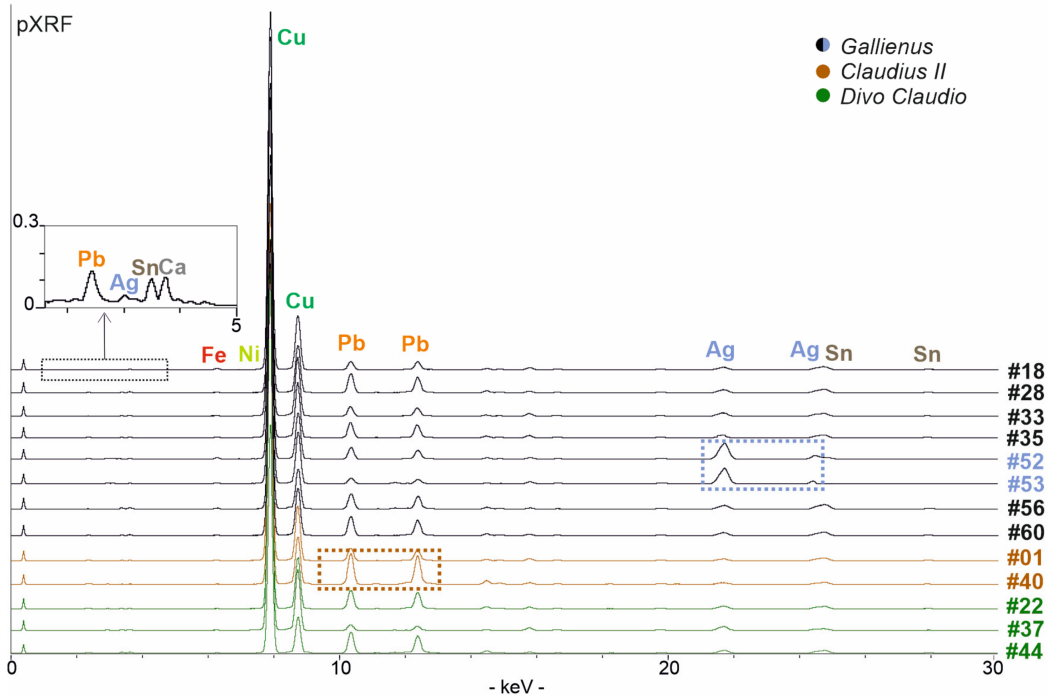

Figure 3. pXRF data of the better-preserved coins (non-visible low KeV peaks are shown in the box above): coins #52 and #53 present a higher content of silver (shown in the blue box) whereas the coin #40 show a higher content of lead (in the brown box).

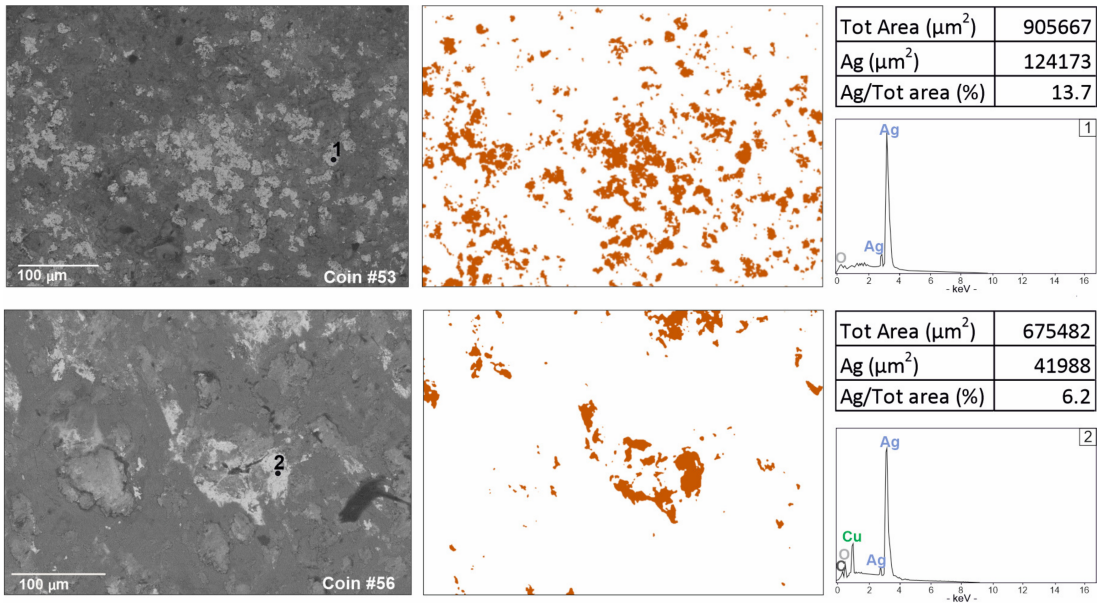

Figure 4. Digital Image Analysis (DIA), obtained by ImageJ segmentation from BSE images, showing in false colour a higher presence of silver in coin #53 against a representative sample with lower silver content (coin #56).

Coins #52 and #53 show a different chemical composition (Figure 3). Coin #52 keeps the same elemental composition but shows a higher silver value; this feature well reflects the composition of the coinage to which the coin belongs to. In fact, the coin refers to a monetary issue from the beginning of Gallienus' single reign for his wife Salonina Augusta. On the other hand, the coin #53 presents a different composition of the alloy. A higher content of silver was detected (Table 2); lead appears in lower contents than the other coins

analysed but, above all, the presence of tin lacks. From the literature data, it is well-known that tin has been added to a greater extent to the alloy in the most degraded series to compensate for the yellowing effects and whiten the silver-poor coin [54]. In this coin, a higher silver content was detected, probably justifying the absence of tin (Table 2). Digital Image Analysis (DIA) was performed on two representative BSE images to support the data obtained from PM2 setting about the difference of silver content (Figure 4). The Ag-rich areas are visible in false colour; a greater distribution of Ag-rich areas in coin #53 is evident compared to the processed image of a representative coin with a lower silver content (coin #56). Segmented areas made it possible to calculate percentage values which appear to be quite consistent with the percentages observed in the PM setting (Table 2; Figure 4). The detected composition of the coin #53 can also be contextualised with historical data. This coin is part of the coins issued by the mint of Mediolanum; that is, the mint that paid the Roman army engaged on the northern borders [65]. In fact, the mint of Mediolanum under Gallienus' empire seems to produce better coins than the mint of Rome, probably to secure the support of the legions, which, in this historical phase, acclaimed the Emperor [66].

4.1.2. *Claudius II* Coins

The coins issued by Emperor Claudius II (coins #1, #40; Figure 2) have a chemical composition, at least in qualitative terms, equivalent to the Gallienus ones. Copper, silver, tin, lead, calcium, iron and nickel were identified by the chemical analyses (Figure 3). The composition of the alloy turns out to be characterised by the presence of the first four elements mentioned above. The chemical analyses revealed a decrease in the silver content compared to Gallienus coins (Table 2), consistent with the lower percentage described in the numismatic literature [55]. In fact, the coinage of Claudius II is defined as the antonianiano nadir, with the lowest silver standards in the history of this Roman silver coinage [67].

Coin #40 (Figure 2) is characterised by a different manufacture; it appears thicker and heavier (ca. 6 g versus 2–3 g of the other analysed coins; Table 1) and presents a higher content of lead (Table 2; Figure 3). Its facture could suggest that this coin was produced by an officina that operated with different manufacturing standards.

4.1.3. *Divo Claudio* Coins

Consecration coins are those issued by Emperors to celebrate the memory of the previous Emperor, in this case Claudius II, and thus legitimise the succession [68]. Among the five consecration coins, three coins issued for Divo Claudio (coins #22, #37, #44 Figure 2) were better preserved and were analysed for this study. Once again, they present a composition qualitatively equivalent to the previous coins analysed. However, it is the least homogeneous group due to the variability of contents of the constituent elements and, in particular, for the lead content (Table 2; Figure 3). This variability can suggest different production workshops or could refer to different issuing authorities. The chemical analyses highlighted that the precious metal content returns to the averages of Gallienus' coinage, testifying that it was recovering from the nadir of the previous coinage [54,67].

4.2. Conservation State

When archaeological artifacts in copper-based alloys degrade, an alteration product called a patina covers the surface layer [13]. The composition and thickness of the patina depend both on the composition of the original alloy and on the environmental conditions in which they are found [69]. Some type of patina can form a compact layer that, for its pleasant appearance, is generally counted among the 'noble' patinas in the literature. In fact, some metals can stop the corrosion processes in the early stages with the formation of surface oxides. These compounds take on the appearance of uniform, adherent and resistant patinas, which isolate and protect the metal from further attacks from the environment.

During the laying, the coins belonging to the treasure of Cumae underwent chemical-physical alterations that affected the composition of the alloy used, modifying the physical

characteristics, the surface and the shape. Thus, various types of patinas are present on the same coin and sometimes on a single face only.

The analysed coins are bronzes with a high presence of lead and a low silver content. These elements tend to form new minerals in contact with the environment through chemical reactions [69]. These mainly include corrosion processes, determined by certain environmental conditions due to elements and compounds such as, for example, water, oxygen and carbon dioxide.

The study began with the observation under a stereomicroscope (up to 11.75×), which made it possible to observe the corroded surfaces and to identify the various patinas. The observed patinas appear in different colours, which are often associated with the presence of newly formed minerals [60]. After the initial observation, X-ray inspection performed by micro-computed tomography was used in a complementary manner to enable detecting hidden damage, such as the internal cracks [69]. Therefore, fractured or chipped coins (#40, #52, #53; Figure 2) were analysed with µ-CT to evaluate the extent of the fracture and consequently the stability of the coin. The crack of sample #53 (Figure 5a) is a real upper crack that crosses the entire thickness of the coin; sample #52 has a crack that radiates from the edge to the centre and that pierces the coin (Figure 5b). The specimen #40 presented a metal gap visible on the only reverse side. Thus, the hole was investigated and small voids that do not pierce the full thickness of the coin were shown, highlighting that the level of corrosion has not yet affected the integrity of the entire specimen (Figure 5c). This information is useful for conservators and for conservation purposes of the treasure. Furthermore, the technique has appeared useful for the classification of coins for numismatic purposes. Due to the poor state of conservation and the non-total legibility, coin #5 (Figure 2) was examined with µ-CT, thanks to which the type on the reverse was clearly identified as a quadripartite altar with a small globe in each box (Figure 5d). Since the image struck on the coins already gives information on the chronology, the identification of this type allowed for a more precise classification of the coin.

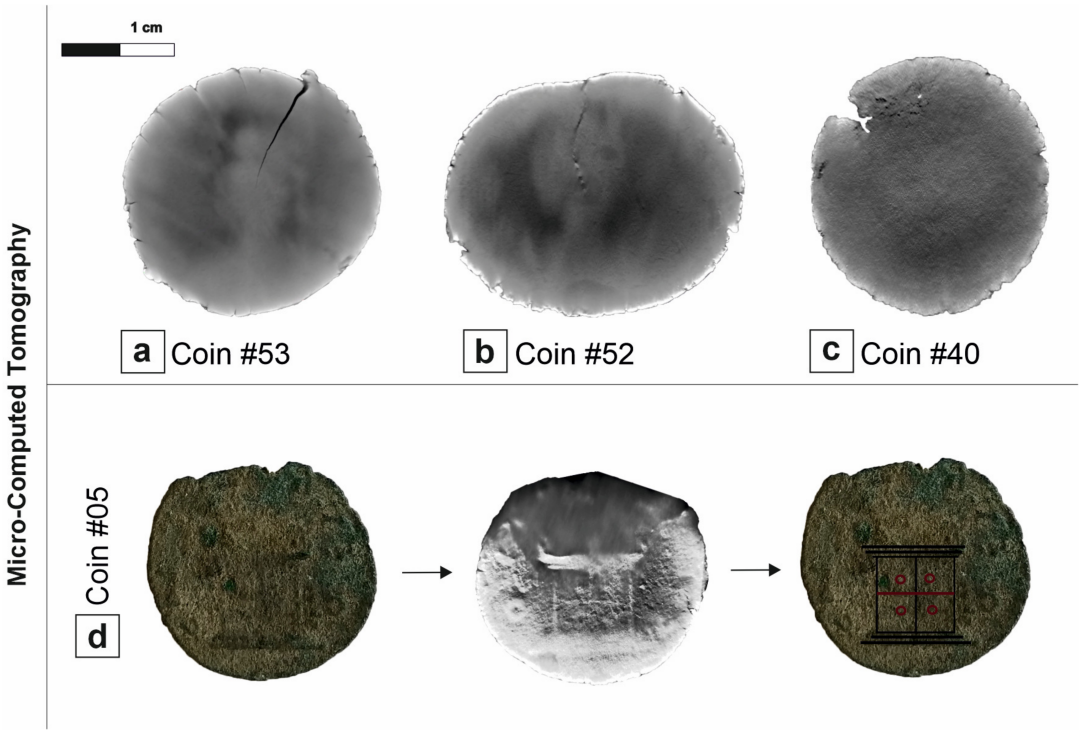

Figure 5. (**a**,**b**) µ-CT images presenting the cracks of the coins #53 and #52; (**c**) slice 501/1004 of the µ-CT images testifying the begin of the corrosion in the coin #40; (**d**) identification of the reverse typology in the high corroded coin #5: the quadripartite altar with small globes returns to visibility in the µ-CT slice.

For the determination of the chemical nature of the corrosion products, a preliminary investigation was carried out with the pXRF analysis (Std. Alloy3 LowZ preset) that showed the presence of copper, iron, calcium, lead, silver, titanium, manganese, silicon, potassium and nickel (Table 3). The light elements not detected with the pXRF analyses were identified with the FESEM-EDS analysis which revealed O, Cl and C in different association with the heavy elements, allowing for the identification of the materials present on the corroded surface. Finally, Raman analyses have returned characteristic spectra of the materials present as corrosion products.

Table 3. Composition of the patinas found on some coins: assignment of mineral by pXRF, FESEM-EDS and Raman spectroscopy results.

Coins	Colour	pXRF	FESEM-EDS	Raman (cm^{-1})	Corrosion Products	Assignment
#01, #30 #33, #44, #56	Red	Cu ***, Pb **, Ag *, Fe *, Ca *, Ti ^{tr}, Mn ^{tr}, Ni ^{tr}	Cu, O	218, 409, 624	Copper oxide	Cuprite
#05, #06, #30, #33, #35, #47, #57, #62	Green	Cu ***, Pb **, Sn *, Ag *, Ca *, Fe *, Ni ^{tr}, Mn ^{tr}, Ti ^{tr}, K ^{tr}	Cu, O, C	265, 350, 430, 525, 1059, 1094	Copper carbonate	Malachite
#05, #41, #57	Whitish	Cu ***, Pb **, Sn *, Ag *, Ca *, Fe *, Ni ^{tr}, Si ^{tr}, P ^{tr}, K ^{tr}	Pb, O, C	220, 1054	Lead carbonate	Cerussite
#30, #37, #47, #52	Green	Cu ***, Pb **, Sn *, Ag *, Mn ^{tr}, K ^{tr}, Ti ^{tr}, Si ^{tr}, Fe ^{tr}, Ni ^{tr}	Cu, Cl, O, P, Al	-	Copper chloride	NI
#05, #52 #62	Yellowish	Cu ***, Pb **, Sn *, Ag *, Fe *, Ni ^{tr}, Si ^{tr}, Ti ^{tr}, Mn ^{tr}, K ^{tr}	Ag, Cl, O	-	Silver chloride	NI

Legend: predominant element (***), medium (**), lower (*), traces (tr), NI (Not Identified).

4.2.1. Oxides Corrosion Products

The processes of formation of corrosion products of metals in archaeological environments have been widely studied. The copper oxidation process begins with the selective dissolution from the α phase of the solid copper solution. During this stage, the dissolved copper reacts with soil anions, such as chloride and carbonate and, therefore, can leave the metal surface. While the copper values decrease, the oxygen content increases significantly. This effect leads to the formation of copper oxides, which appears as a red-brown patina [13].

The red patina (Figure 6a) on the coin surface was studied by scanning electron microscopy, which showed a radiated structure composed of crystals from the acicular habit (Figure 6b) and revealed high copper and oxygen detected by EDS analyses (Figure 6c). As already observed in optical microscope images (Figure 6a,c), the patina is localised in correspondence with some depressions and, therefore, it is below the others. Copper oxides thus comprise the first oxidation layer that is closest to the alloy itself. The identification of the resulting corrosion product was achieved by Raman analysis, which detected peaks at 218, 409 and 624 cm^{-1} (Table 3) attributable to cuprous oxide, namely, cuprite (Cu_2O) (Figure 6d) [70].

4.2.2. Carbonates Corrosion Products

Another element that contributes to modifying the original composition of the coins is carbon: carbon dioxide, conveyed by humidity, gives rise to compounds that we see as corrosion patinas on the analysed coins.

Most of the corroded coins presented a green patina (Figure 7a). The mamillary or botryoidal texture of this corrosion product was investigated via optical and electron microscopes at various magnifications (Figure 7b). In EDS analyses, this green area presented carbon in association with oxygen and copper (Figure 7c). Raman analyses have identi-

fied the presence of a copper carbonate with peaks at 265, 350, 430, 525, 1059, 1094 cm^{-1} attributable to the malachite ($Cu_2CO_3(OH)_2$) (Figure 7d; Table 3)) [58].

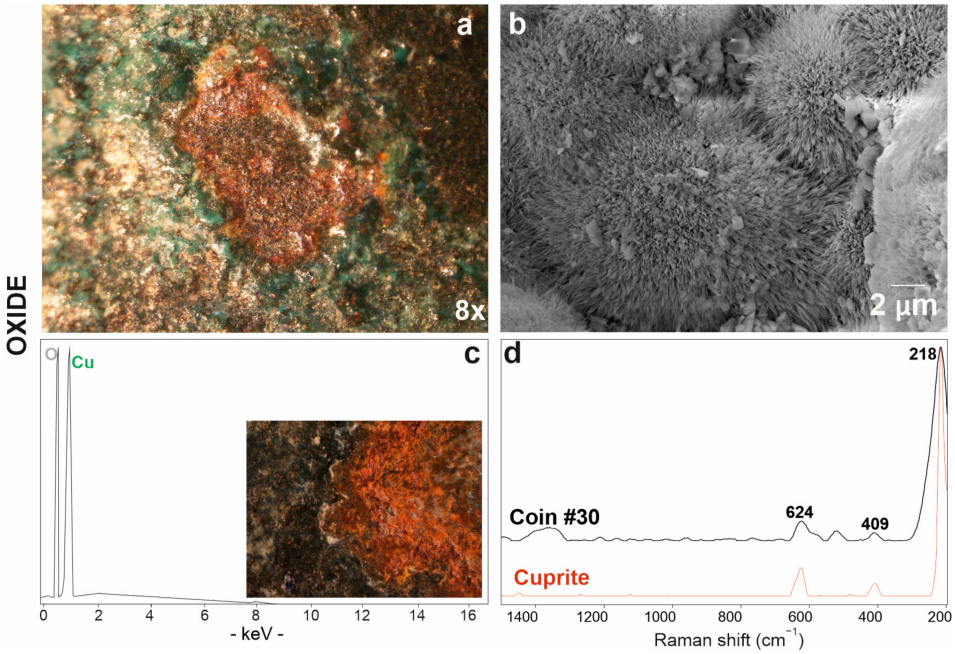

Figure 6. Red patina of copper oxide investigated via optical (**a**) and electronic microscope SE (secondary electron) image (**b**) with EDS spectrum (**c**); (**d**) Raman spectrum of coin #30 (in black) and RRUFF database reference spectrum of the cuprite mineral (in red).

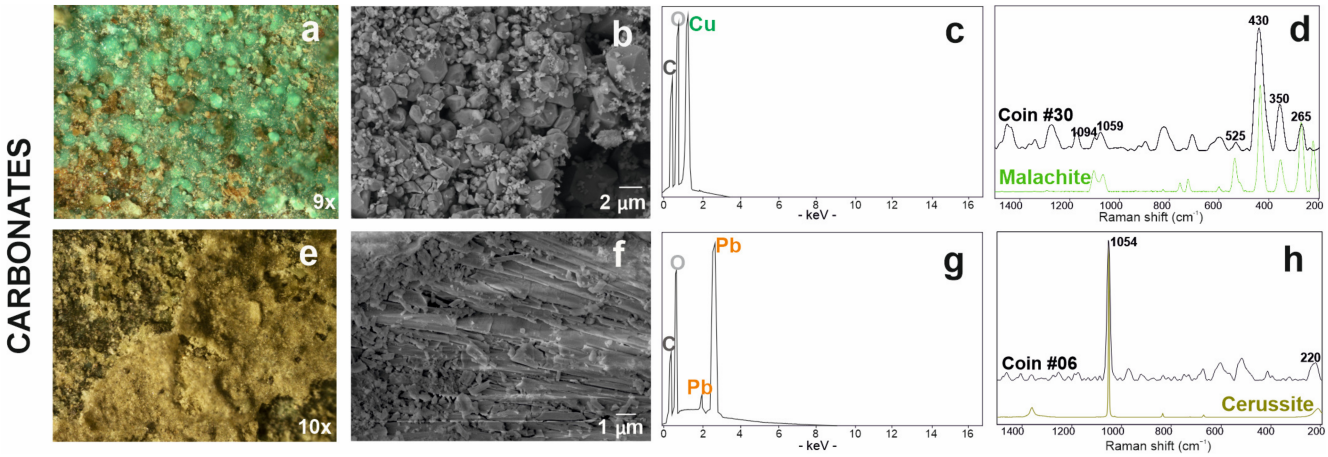

Figure 7. Carbonate-based patinas: the copper carbonate is presented with the stereomicrograph (**a**), the SE image (**b**) and the related EDS microanalysis spectrum (**c**), finally with the Raman spectrum acquired on the coin # 30 (in black) and malachite reference spectrum (in green) from the RUFF database (**d**); similarly, lead carbonate is presented with the stereomicrograph (**e**), the SE image (**f**) and the related EDS microanalysis spectrum (**g**); finally with the Raman spectrum acquired on coin #06 (in black) and cerussite reference spectrum (in green) from the RUFF database (**h**).

A whitish-yellowish patina, which often covered the green ones, was observed under stereomicroscope (Figure 7e) and electron microscope (Figure 7f); in this area, the FESEM-EDS analyses showed the presence of carbon, oxygen and lead (Figure 7g). On this surfaces, Raman spectroscopic analysis identified the presence of a lead carbonate with the characteristic peaks of cerussite ($PbCO_3$) at 220 and 1054 cm^{-1} (Figure 7h; Table 3) [71].

The Raman spectra on the surface of coin #53 also provided information about the presence of carbon black (Figure S1a), a compound that derives from the combustion of organic material [72]. This may suggest that the coins have been in contact with burnt organic material at an unspecified stage of their existence. Furthermore, the presence of material of organic origin was identified by high resolution FESEM investigation (5700×) in filaments of submicrometric thickness, giving us information on the presence of some microorganisms (Figure S1b). These organic components were found on coin #52 and are probably due to fungi or cellulose.

4.2.3. Chlorides Corrosion Products

Chloride-based corrosion products have been detected in coins #5, #30, #41 and #52 (Figure 2). The patina of corrosion is light green in colour (Figure 8a) and has a dusty appearance. This type of patina consists of copper, chlorine and traces of oxygen, aluminium and phosphorous (Figure 8b,c; Table 3) but, unfortunately, it was not identified by Raman spectroscopy. The formation of chlorides on the surface of a buried metal product is due to a humid or saline underground environment [18,73]. The chlorine ion attacks the copper from its oxides or carbonates transforming it into cuprous chloride and for this reason they often stratify on the surface of the coin [74]. In fact, copper chloride was found together with other copper corrosion products, carbonates (malachite) and oxides (cuprite). These data could be consistent with Cuman soil, which is found in close proximity to the sea. In fact, soils with an acid pH support the formation of binary salts present in these chloride-based alteration products [60,75,76].

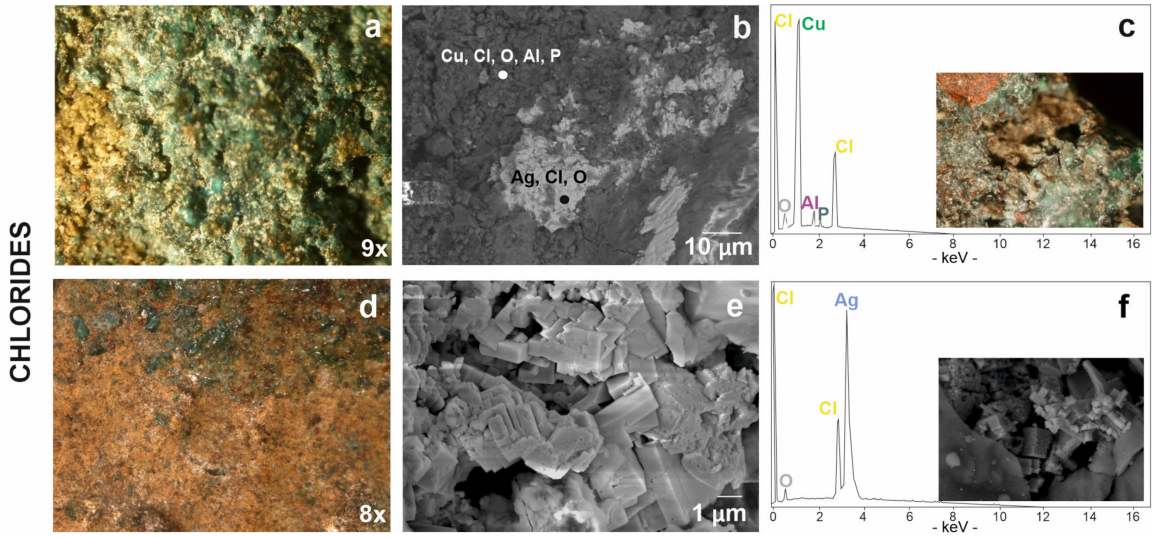

Figure 8. Chloride-based patinas from stereomicroscopy to scanning electron microscopy: (**a**) chlorine associated to copper visible in a green product of corrosion, (**b**) in dark grey areas in BSE image and (**c**) relative EDS spectrum with the stereomicrograph of degraded area by chlorine on coin #30 in the box; (**d**) chlorine associated to silver visible in a yellowish patina, (**e**) in cubic structure in SE image and (**f**) relative EDS spectrum with SE image of silver-chloride in the box.

These corrosion phenomena are generally localised, but they can reach the whole coin and create serious problems for the stability of the item. In fact, due to the hydrolysis effect, cuprous chloride can give rise to the so-called "bronze disease", producing basic copper chlorides and causing breakage or fragmentation [74]. Pitting was found in only one instance on the outer surface of the #30 coin (Figure 8c). Here, the corrosion process is in an advanced state; the original surface has been damaged, making the coin legends difficult to read. The presence of these patinas indicates a potential threat if the artifacts are exposed to environments with high humidity and abundant oxygen supply; it becomes important information for intervening on the conservation of the artifact.

In addition to copper, chlorine also seems to be associated to silver. In fact, another type of yellowish patina (Figure 8d) showed an inhomogeneous surface with deformations and volume growth in some points. This yellowish surface was investigated by FESEM analyses showing a characteristic cubic morphology (Figure 8e,f) and revealed the composition of silver chloride including traces of oxygen (Figure 8f).

The silver mineralisation process of the archaeological buried object begins with the absorption of oxygen molecules which are transformed into oxygen ions [77]. With the high humidity and in a chloride rich environment, the objects can be completely transformed in silver chloride [78]. However, the mineral constituting the corrosion product was not identified by Raman analysis.

5. Conclusions

The methodological approach based on non-destructive and non-invasive techniques allowed us to obtain information on the chemical composition of the better-preserved coins of the whole treasure and on corrosion products in order to preserve the archaeological artefacts from further damage.

The coins analysed in this study belong to a critical period of the Roman imperial coinage, when the silver coin suffered a significant debasement. In fact, the lead–bronze alloy shows very low contents of silver and some differences between the various Roman mint issues. The content of silver seems to be lower in the coins of Claudius II than in the issues of Gallienus and in those for Divo Claudio. Among Gallienus' coins, two exceptions corroborate the historical sources according to which, in this antoninianus phase, certain issues presented a higher precious metal amount. Furthermore, the mint of Mediolanum, under Gallienus control, produced coins with a metallic spindle in which tin was absent. The content of silver is higher in this example and in the Roman mint coin minted for Salonina Augusta.

Although some coins are in a good state of conservation, other coins have heterogeneous patinas on at least one side and fractures that cross the entire thickness. The occasional presence of oxide-based corrosion patinas, if in a controlled environment, does not represent a serious problem for the conservation of the find since these can inhibit the progress of the corrosion process by protecting the metal underneath; quite the opposite: in humid environments, the cuprous oxide will ruin the integrity of the coin. However, a copper carbonate appears to be the major corrosion compound on the surfaces of the coins analysed. Other more aggressive chloride-based patinas, on the other hand, inform of the poor state of conservation of the coins and suggest appropriate restoration and conservation interventions to prevent the coins from becoming completely illegible. Macroscopic and microscopic observations of the surface of all the coins suggest that the formation of corrosion products is quite heterogeneous even on coins of similar chemical composition and coming from the same stratigraphic unit and from the same closed context. In fact, with the same chemical composition of the alloy, the univocal correspondence between the burial environment and the corrosion products does not always occur, probably due to different micro-environments that influenced the formation mechanisms of alteration products [79].

Supplementary Materials: The following supporting information can be downloaded at: https://www.mdpi.com/article/10.3390/heritage6020110/s1, Figure S1: (a) presence of carbon black on the coin #53; (b) microorganisms found on the coin #52.

Author Contributions: Conceptualisation, S.P., G.B., E.S. and A.D.B.; methodology, S.P., G.B., L.P. and A.D.B.; formal analysis, S.P., G.B., C.G. (Chiara Germinario), C.G. (Celestino Grifa), F.I., M.M. and M.V.; investigation, S.P., G.B., C.G. (Chiara Germinario), C.G. (Celestino Grifa), F.I., M.M., L.P., E.S., M.V. and A.D.B.; data curation, S.P.; writing—original draft, S.P.; writing—review and editing, all authors; visualisation, S.P.; resources, P.M. and E.S.; validation, all authors; supervision, C.G. (Celestino Grifa) and A.D.B. All authors have read and agreed to the published version of the manuscript.

Funding: This research received no external funding.

Data Availability Statement: The data presented in this study are available on request from the corresponding author.

Acknowledgments: The authors are grateful to Fabio Pagano, Director of Parco Archeologico dei Campi Flegrei, for providing the necessary authorisation for sampling and analyses, to Marcella Leone for her help in providing the samples and to Roberto de Gennaro for his valuable support in the FESEM-EDS investigation.

Conflicts of Interest: The authors declare no conflict of interest.

References

1. Blet-Lemarquand, M.; Ponting, M.J. Scientific and technical application. A survey of numismatic research 2002–2007. In *The International Numismatic Commission*; Amandry, M., Bateson, D., Eds.; International Association of Professional Numismatists: Glasgow, UK, 2009; pp. 714–720.
2. Linke, R.; Schreiner, M.; Demortier, G.; Alram, M. Determination of the provenance of medieval silver coins: Potential and limitations of x-ray analysis using photons, electrons or protons. *X-Ray Spectrom.* **2003**, *32*, 373–380. [CrossRef]
3. Gondonneau, A.; Guerra, M.F. The circulation of precious metals in the Arab Empire: The case of the near and the Middle East. *Archaeometry* **2002**, *44*, 573–599. [CrossRef]
4. Clay, T. Metallurgy and Metallography in Numismatic. *Numis e Antich Class* **1988**, *17*, 341–352.
5. Rehren, T.; Pernicka, E. Coins, Artefacts and isotopes-archaeometallurgy and Archaeometry. *Archaeometry* **2008**, *50*, 232–248. [CrossRef]
6. Morrison, C.; Barrandon, J.N.; Brenot, C. Composition and technology of ancient and medieval coinages: A reassessment of analytical results. *Mus. Notes (Am. Numis. Soc.)* **1987**, *32*, 181–209.
7. Gitler, H.; Ponting, M.J. Rome and the east a study of the chemical composition of roman silver coinage during the reign of Septimius Severus ad 193–211. *Topoi* **2007**, *8*, 375–397.
8. Elayi, A.G.; Barrandon, J.-N.; Elayi, J. The Devaluation of Sidonian Silver Coinage in 365 BCE and the First Bronze Issues. *Am. J. Numis.* **2007**, *19*, 1–8.
9. Butcher, K.; Ponting, M. The Roman denarius under the Julio-Claudian Emperors: Mints, metallurgy and technology. *Oxford J. Archaeol.* **2005**, *24*, 163–197. [CrossRef]
10. Pearson, P.N.; Botticelli, M.; Ericsson, J.; Olender, J.; Spruženiece, L. Authenticating coins of the 'Roman Emperor' Sponsian. *PLoS ONE* **2022**, *17*, e0274285. [CrossRef]
11. Caley, E.R. Klaproth as a pioneer in the chemical investigation of antiquities. *J. Chem. Educ.* **1949**, *26*, 242. [CrossRef]
12. Rizzo, F.; Cirrone, G.P.; Cuttone, G.; Esposito, A.; Garraffo, S.; Pappalardo, G.; Pappalardo, L.; Romano, F.P.; Russo, S. Non-destructive determination of the silver content in Roman coins (nummi), dated to 308–311 A.D., by the combined use of PIXE-alpha, XRF and DPAA techniques. *Microchem. J.* **2011**, *97*, 286–290. [CrossRef]
13. Robbiola, L.; Blengino, J.M.; Fiaud, C. Morphology and mechanisms of formation of natural patinas on archaeological Cu-Sn alloys. *Corros. Sci.* **1998**, *40*, 2083–2111. [CrossRef]
14. Reale, R.; Plattner, S.H.; Guida, G.; Sammartino, M.P.; Visco, G. Ancient coins: Cluster analysis applied to find a correlation between corrosion process and burial soil characteristics. *Chem. Cent. J.* **2012**, *6*, 52–59. [CrossRef]
15. Beck, L.; Bosonnet, S.; Réveillon, S.; Eliot, D.; Pilon, F. Silver surface enrichment of silver–copper alloys: A limitation for the analysis of ancient silver coins by surface techniques. *Nucl. Instrum. Methods Phys. Res. Sect. B Beam Interact. Mater. Atoms.* **2004**, *226*, 153–162. [CrossRef]
16. Caridi, F.; Mezzasalma, A.M.; Castrizio, E.D. An investigation on the patina of ancient bronze coins. *Radiat. Eff. Defects Solids* **2014**, *169*, 371–379. [CrossRef]
17. Vadrucci, M.; Mazzinghi, A.; Gorghinian, A.; Picardi, L.; Ronsivalle, C.; Ruberto, C.; Chiari, M. Analysis of Roman Imperial coins by combined PIXE, HE-PIXE and μ-XRF. *Appl. Radiat. Isot.* **2019**, *143*, 35–40. [CrossRef]
18. Crosera, M.; Baracchini, E.; Prenesti, E.; Giacomello, A.; Callegher, B.; Oliveri, P.; Adami, G. Elemental characterization of surface and bulk of copper-based coins from the Byzantine-period by means of spectroscopic techniques. *Microchem. J.* **2019**, *147*, 422–428. [CrossRef]
19. Longoni, A.; Fiorini, C.; Leutenegger, P.; Sciuti, S.; Fronterotta, G.; Strüder, L.; Lechner, P. A portable XRF spectrometer for non-destructive analyses in archaeometry. *Nucl. Instrum. Methods Phys. Res. Sect. A Accel. Spectrometers Detect. Assoc. Equip.* **1998**, *409*, 407–409. [CrossRef]
20. Scuotto, M.; Bassi, C.; Lezzerini, M.; Grifoni, E.; Legnaioli, S.; Lorenzetti, G.; Pagnotta, S.; Palleschi, V. X-ray fluorescence analysis on a group of coins from the ancient roman city of Tridentum (Trento, Italy). *X-Ray Spectrom.* **2014**, *43*, 370–374. [CrossRef]
21. Pardini, L.; El Hassan, A.; Ferretti, M.; Foresta, A.; Legnaioli, S.; Lorenzetti, G.; Nebbia, N.; Catalli, F.; Harith, M.H.; Diaz Pace, D.; et al. X-ray fluorescence and laser-induced breakdown spectroscopy analysis of Roman silver denarii. *Spectrochim. Acta Part B At. Spectrosc.* **2012**, *74–75*, 156–161. [CrossRef]

22. Corsi, J.; Lo Giudice, A.; Re, A.; Agostino, A.; Barello, F. Potentialities of X-ray fluorescence analysis in numismatics: The case study of pre-Roman coins from Cisalpine Gaul. *Archaeol. Anthropol. Sci.* **2018**, *10*, 431–438. [CrossRef]
23. Ferretti, M. The investigation of ancient metal artefacts by portable X-ray fluorescence devices. *J. Anal. At. Spectrom.* **2014**, *29*, 1753–1766. [CrossRef]
24. Šatović, D.; Desnica, V.; Fazinić, S. Use of portable X-ray fluorescence instrument for bulk alloy analysis on low corroded indoor bronzes. *Spectrochim. Acta Part B At. Spectrosc.* **2013**, *89*, 7–13. [CrossRef]
25. Robotti, S.; Rizzi, P.; Soffritti, C.; Garagnani, G.L.; Greco, C.; Facchetti, F.; Borla, M.; Operti, L.; Agostino, A. Reliability of portable X-ray Fluorescence for the chemical characterisation of ancient corroded copper-tin alloys. *Spectrochim. Acta Part B At. Spectrosc.* **2018**, *146*, 41–49. [CrossRef]
26. Sebar, L.E.; Iannucci, L.; Goren, Y.; Fabian, P.; Angelini, E.; Grassini, S. Raman investigation of corrosion products on Roman copper-based artefacts. *Acta IMEKO* **2020**, *10*, 129–135. [CrossRef]
27. Bertolotti, G.; Bersani, D.; Lottici, P.P.; Alesiani, M.; Malcherek, T.; Schlüter, J. Micro-Raman study of copper hydroxychlorides and other corrosion products of bronze samples mimicking archaeological coins. *Anal. Bioanal. Chem.* **2012**, *402*, 1451–1457. [CrossRef]
28. Orlić, N.; Jelovica, I.; Dobrinić, J.; Lofrumento, C.; Salvi, P.R. Analysis of ancient and medieval specimens using nondestructive spectroscopic techniques. *Nucl. Instrum. Methods Phys. Res. Sect. A Accel. Spectrometers Detect. Assoc. Equip.* **2007**, *580*, 739–742. [CrossRef]
29. Ingo, G.M.; Riccucci, C.; Pascucci, M.; Messina, E.; Giuliani, C.; Biocca, P.; Tortora, L.; Fierro, G.; Di Carlo, G. Combined use of FE-SEM+EDS, ToF-SIMS, XPS, XRD and OM for the study of ancient gilded artefacts. *Appl. Surf. Sci.* **2018**, *446*, 168–176. [CrossRef]
30. Mezzi, A.; Riccucci, C.; De Caro, T.; Angelini, E.; Faraldi, F.; Grassini, S.; Gouda, V.K. Combined use of SA-XPS, XRD and SEM-EDS for the micro-chemical characterisation of Ag-based archaeological artefacts. *Surf. Interface Anal.* **2014**, *46*, 801–806. [CrossRef]
31. Di Fazio, M.; Felici, A.C.; Catalli, F.; De Vito, C. Microstructure and chemical composition of Roman orichalcum coins emitted after the monetary reform of Augustus (23 B.C.). *Sci. Rep.* **2019**, *9*, 12668. [CrossRef]
32. Doménech-Carbó, M.T.; Di Turo, F.; Montoya, N.; Catalli, F.; Doménech-Carbó, A.; De Vito, C. FIB-FESEM and EMPA results on Antoninianus silver coins for manufacturing and corrosion processes. *Sci. Rep.* **2018**, *8*, 10676. [CrossRef]
33. Di Turo, F.; Coletti, F.; De Vito, C. Investigations on alloy-burial environment interaction of archaeological bronze coins. *Microchem. J.* **2020**, *157*, 104882. [CrossRef]
34. Doménech-Carbó, A.; Donnici, M.; Álvarez Romero, C.; Daniele, S.; Doménech-Carbó, M. Multiple-scan voltammetry of immobilized particles of ancient copper/bronze coins. *J. Solid State Electrochem.* **2021**, *25*, 195–206. [CrossRef]
35. Serghini-Idrissi, M.; Bernard, M.C.; Harrif, F.Z.; Joiret, S.; Rahmouni, K.; Srhiri, A.; Takenouti, H.; Vivier, V.; Ziani, M. Electrochemical and spectroscopic characterizations of patinas formed on an archaeological bronze coin. *Electrochim. Acta* **2005**, *50*, 4699–4709. [CrossRef]
36. Es Sebar, L.; Parvis, M.; Grassini, S.; Angelini, E. Monitoraggio dello stato di conservazione delle opere d'arte della Collezione Gori. *La Metall. Ital.* **2020**, *12*, 73–77.
37. Pagano, F.; Del Villano, M. *Terra. La scultura di un paesaggio*; Gangemi Editore International: Rome, Italy, 2022.
38. Scott, D.A.; Oddy, A. *Copper and Bronze in Art: Corrosion, Colorants, Conservation*; The Getty Conservation Institute: Los Angeles, CA, USA, 2002.
39. Gasparri, C.; Greco, G. *Cuma. Indagini Archeologiche e Nuove Scoperte, Atti Della Giornata di Studi (Napoli, 12 Dicembre 2007)*; Quad del Cent Stud Magna Grecia Stud Cumani: Naples, Italy, 2009.
40. Brun, J.P.; Munzi, P. *La Necropoli Monumentale in Età Romana a Nord Della Città di Cuma*; Cuma Atti del quarantaquattresimo convegno di Studi sulla Magna Grecia: Taranto, Italy, 2009; pp. 635–718.
41. Brun, J.-P.; Munzi, P.; Conca, E.; Covolan, M.; de Rosa, S.; Mastro, B.D.; Lemaire, B.; Leone, M.; Sachau-Carcel, G. La necropoli ellenistica di Cuma presso la Porta mediana. Le ricerche del Centre Jean Bérard. Campagne di scavo 2017–2018. *Puteoli Cumae Misenum. Riv. Di Studi E Not. Del Parco Archeol. Dei Campi Flegrei* **2021**, *3*, 244–270.
42. Brun, J.P.; Munzi, P.; Botte, E. Cuma. Il monumento funerario della "Sfinge" (A63) nella necropoli della Porta mediana. In *Complessi Monum e Arred scultoreo nella Reg I Latium Camp Nuove scoperte e Propos di Lett contesto, Atti del convegno internazionale, Dicembre 2013, Napoli, Italy*; Capaldi, C., Ed.; Naus Editoria: Naples, Italy, 2018; pp. 121–148.
43. Germinario, C.; Cultrone, G.; Cavassa, L.; De Bonis, A.; Izzo, F.; Langella, A.; Mercurio, M.; Morra, V.; Munzi, P.; Grifa, C. Local production and imitations of Late Roman pottery from a well in the Roman necropolis of Cuma in Naples, Italy. *Geoarchaeology* **2019**, *34*, 62–79. [CrossRef]
44. Spagnoli, E. Monete a Cuma nel III sec d.C.: Un ripostiglio monetale e altre evidenze. In *Pre-Atti Incontr Internazionale di Stud Cuma e i Campi Flegrei Archeol Storia Soc Territ (Napoli-Pozzuoli, 11–13 Maggio 2022)*; Capaldi, C., Valente, I., Eds.; Naus Editore: Naples, Italy, 2022; p. 23.
45. Cavassa, L.; Munzi, P.; Brun, J.P.; Botte, E.; Germinario, C.; Grifa, C.; Langella, A.; Morra, V.; Mercurio, M. Cumes. Le matériel tardo-antique découvert dans un puits: Entre données typologiques et analyses archéométriques. In *LRCW 5-1—Late Rom Coarse Wares, Cook Wares Amphor Mediterr Archaeol Archaeom. Alexandria*; Dixneuf, D., Ed.; Centre d'Études Alexandrines: Alexandria, Egypt, 2018; pp. 385–405.

46. Brun, J.-P.; Munzi, P.; Chapelin, G.; Covolan, M.; Lemaire, B.; Leone, M.; Géraldine, S.-C. Recherches archéologiques dans la nécropole de la Porte médiane à Cumes. *Chron des Act archéologiques l'École française Rome* **2017**. [CrossRef]
47. Cavassa, L.; Coubray, S.; Mannocci, E.; Oboussier, A.; Pawlowicz, M.; Rosa, C.; Turci, M. Recherches sur la production céramique à Pompéi: L'atelier des lampes à huile (Reg. I, Ins. 20, 2-3). Campagne 2017. *Chron des Act Archéologiques l'École française Rome* **2018**. [CrossRef]
48. Augustae, S.H.; The Perfect Library. *Historia Augusta*; CreateSpace Independent Publishing Platform: Scotts Valley, CA, USA, 2014.
49. Bland, R. From Gordian III to the Gallic Empire (AD 238–274). In *The Oxford Handbook of Greek and Roman Coinage*; Metcalf, W.E., Ed.; Oxford University Press: Oxford, UK, 2012; pp. 514–537.
50. Estiot, S. The Later Third Century. In *The Oxford Handbook of Greek and Roman Coinage*; Metcalf, W.E., Ed.; Oxford University Press: Oxford, UK, 2012; pp. 538–560.
51. Peachin, M. *Roman Imperial Titulature and Chronology, A.D. 235–284*; Gieben Publisher: Amsterdam, The Netherlands, 1990.
52. Lo Cascio, E. La dimensione finanziaria e monetaria della crisi del III secolo d.C. *Stud. Stor. Fond. Ist Gramsci.* **1984**, *1*, 161–202.
53. Barello, F. L'Impero Romano in crisi. L'Italia nord-occidentale. Aspetti monetari. Un confronto Dramm con XXI secolo l'Impero Rom del III secolo nella Cris Mone. In *Atti del Convegno a Biassono (9 Giugno 2012)*; Museo Civico Carlo Verri: Biassono, Italy, 2014; pp. 81–92.
54. Cope, L.H. *The Metallurgical Development of the Roman Imperial Coinage during the First Five Centuries d.C.*; Liverpool Polytech: Liverpool, UK, 1974.
55. Cope, L.H. The nadir of the imperial antoninianus in the reign of Claudius II Gothicus, A.D. 268–270. *Numis. Chron.* **1969**, *9*, 145–161.
56. Conti, C.; Botteon, A.; Bertasa, M.; Colombo, C.; Realini, M.; Sali, D. Portable Sequentially Shifted Excitation Raman spectroscopy as an innovative tool for in situ chemical interrogation of painted surfaces. *Analyst* **2016**, *141*, 4599–4607. [CrossRef] [PubMed]
57. Lafuente, B.; Downs, R.T.; Yang, H.; Stone, N. The power of databases: The RRUFF project. In *Highlights in Mineralogical Crystallography*; De Gruyter: Berlin, Germany, 2015; pp. 1–30.
58. Bouchard, M.; Smith, D.C. Catalogue of 45 reference Raman spectra of minerals concerning research in art history or archaeology, especially on corroded metals and coloured glass. *Spectrochim. Acta Part A Mol. Biomol. Spectrosc.* **2003**, *59*, 2247–2266. [CrossRef] [PubMed]
59. Giumlia-Mair, A. On surface analysis and archaeometallurgy. *Nucl. Instrum. Methods Phys. Res. Sect. B Beam. Interact. Mater. Atoms* **2005**, *239*, 35–43. [CrossRef]
60. Giardino, C. *I Metalli Nel Mondo Antico, Introduzione All'archeometallurgia*; Manuali Laterza: Rome, Italy, 2010.
61. Rackham, H. *Pliny the Elder. Natural History in Ten Volumes*; Loeb Classical Library: Cambridge, UK, 1968.
62. Craddock, P.T.; Meeks, N.D. Iron in Ancient Copper. *Archaeometry* **1987**, *29*, 187–204. [CrossRef]
63. Cope, L.H. The fineness and sequence of the Gallienic antoniniani, A.D. 259-68. *Numis Chron.* **1977**, *17*, 216–219.
64. Besly, E.M.; Bland, R.F. *The Cunetio Treasure. Roman Coinage of the Third Century AD*; British Museum Press: London, UK, 1983.
65. Laffranchi, L. Le monete legionarie dell'Imperatore Gallieno e la sua terza grande vittoria. *Riv Ital di Numis e Sci Affin* **1941**, *1*, 3–15.
66. de Blois, L. *The Policy of the Emperor Gallienus*; Brill, E.J., Ed.; Studies of the Dutch Archaeological and Historical Society: Leiden, The Netherlands, 1976.
67. Cope, L.H.; King, C.E.; Northover, J.P.; Clay, T. *Metal Analyses of Roman Coins Minted Under the Empire*; The British Museum: London, UK, 1997.
68. Lo Monaco, V. Le monete di consacrazione di Claudio II il Gotico. In *Il tesoro dei sei Imperatori dalla baia di Camarina*; Guzzetta, G., Ed.; Monografie della Scuola di Specializzazione in Beni Archeologici dell'Università degli Studi di Catania: Catania, Italy, 2014; pp. 127–130.
69. Oudbashi, O.; Wanhill, R. Long-term embrittlement of ancient copper and silver alloys. *Heritage* **2021**, *4*, 2287–2319. [CrossRef]
70. de Caro, T.; Angelini, E.; Sebar, L.E. Application of μ-Raman spectroscopy to the study of the corrosion products of archaeological coins. *Acta IMEKO* **2021**, *10*, 234–240. [CrossRef]
71. Burgio, L.; Clark, R.J.H. Library of FT-Raman spectra of pigments, minerals, pigment media and varnishes, and supplement to existing library of Raman spectra of pigments with visible excitation. *Spectrochim. Acta Part A Mol. Biomol. Spectrosc.* **2001**, *57*, 1491–1521. [CrossRef]
72. Tomasini, E.P.; Halac, E.B.; Reinoso, M.; Di Liscia, E.J.; Maier, M.S. Micro-Raman spectroscopy of carbon-based black pigments. *J. Raman Spectrosc.* **2012**, *43*, 1671–1675. [CrossRef]
73. Scott, D.A. Bronze disease: A review of some chemical problems and the role of relative humidity. *J. Am. Inst. Conserv.* **1990**, *29*, 193–206. [CrossRef]
74. Organ, R.M. Aspects of bronze patina and its treatment. *Stud. Conserv.* **1963**, *8*, 1–9. [CrossRef]
75. Papadopoulou, O.; Vassiliou, P.; Grassini, S.; Angelini, E.; Gouda, V. Soil-induced corrosion of ancient Roman brass—A case study. *Mater. Corros.* **2016**, *67*, 160–169. [CrossRef]
76. Oudbashi, O. A methodological approach to estimate soil corrosivity for archaeological copper alloy artefacts. *Herit. Sci.* **2018**, *6*, 2. [CrossRef]

77. Novakovic, J.; Vassiliou, P. Corrosion of silver alloy artefacts in soil. In Proceedings of the International Conference on Conservation Strategies for Saving Indoor Metallic Collections with a Special Section on Legal Issues in the Conservation of Cultural Heritage, Cairo, Egypt, 26–28 February 2007; TEI of Athens: Cairo, Egypt; pp. 58–63.
78. Marchand, G.; Guilminot, E.; Lemoine, S.; Rossetti, L.; Vieau, M.; Stephant, N. Degradation of archaeological horn silver artefacts in burials. *Herit. Sci.* **2014**, *2*, 5. [CrossRef]
79. Pronti, L.; Felici, A.C.; Alesiani, M.; Tarquini, O.; Bracciale, M.P.; Santarelli, M.L.; Pardini, G.; Piacentini, M. Characterisation of corrosion layers formed under burial environment of copper-based Greek and Roman coins from Pompeii. *Appl. Phys. A* **2015**, *121*, 59–68. [CrossRef]